Journal of Molecular Spectroscopy 405 (2024) 111949

Contents lists available at ScienceDirect

Journal of Molecular Spectroscopy

journal homepage: www.elsevier.com/locate/yjmsp

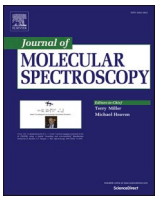

Microwave spectrum and molecular structure calculations for η^4-butadiene ruthenium tricarbonyl

Adam M. Daly [a], Kristen K. Roehling [a], Rhett P. Hill [a], Myla G. Gonzalez [a], Xin Kang [b], Lisa McElwee-White [b], Stephen G. Kukolich [a,*]

[a] Department of Chemistry and Biochemistry, University of Arizona, 1306 University Avenue, Tucson AZ 85721, USA
[b] Department of Chemistry, University of Florida, Gainesville, FL 32611-7200, USA

A B S T R A C T

The microwave spectrum of η^4-butadiene ruthenium tricarbonyl was measured in the 5–15 GHz frequency range using a Flygare-Balle type pulsed beam Fourier transform microwave (FTMW) spectrometer. The rotational constants for the ^{102}Ru isotopologue were determined to have the following values: A = 932.20099(42), B = 858.03248(47) and C = 831.35161(37) MHz. The centrifugal distortion constant d_J is 0.0862(29)kHz. 22 a-dipole and 4c-dipole transitions were measured. Extensive high-level G16 calculations were made using DFT and MP2 methods with various basis sets, some including core-potentials (ECP). The best structure was calculated with Gaussian 16 using B3LYP/def2-QZVPP, which includes a core potential (ECP). Extensive all-electron calculations were made based on the best ECP structure to predict ^{101}Ru and ^{99}Ru quadrupole coupling strengths. Quadrupole hyperfine structure splittings were measured for both ^{101}Ru and ^{99}Ru. The hyperfine structure splittings for the ^{101}Ru nuclear quadrupole were measured, yielding the values of $1.5\chi_{aa}$ = 98.12(17) MHz and $0.25(\chi_{bb}\text{-}\chi_{cc})$ = 36.059(30). Measured hyperfine structure splittings for ^{99}Ru quadrupole coupling yielded the values of $1.5\chi_{aa}$ = 16.99(77) MHz and $0.25(\chi_{bb}\text{-}\chi_{cc})$ = 6.23(32). These values are in reasonable agreement with some of the all-electron calculations.

1. Introduction

This paper presents the first gas-phase structural data on the organometallic complex, (η^4-1,3-butadiene)Ru(CO)$_3$, and first gas-phase molecular quadrupole coupling data for ^{101}Ru and ^{99}Ru. The rotational transitions were measured in the 5 to 16 GHz range using a Flygare-Balle type spectrometer [1] and analyzed with the Pickett programs [2].

Ruthenium has been of practical interest as a material for fabrication of integrated circuits [3,4,5,6] and, as a result, its complexes have been investigated as precursors [7,8] for deposition of metal films and nanostructures. As an example, the transition metal complex butadiene ruthenium tricarbonyl has been used for atomic layer deposition of Ru-containing films [9] and has been evaluated as a precursor for photo-assisted chemical vapor deposition of metal films on self-assembled monolayers. [10].

Hallam and Pauson commented on the unusual stability and provided a correct basic structure for butadiene iron tricarbonyl in 1958. [11] The stability was associated with the η^4 π-facial bonding similar to the much better-known η^5 π-facial bonding of the cyclopentadienyl rings in the ferrocene structure elucidated by Wilkinson, et al. in 1952. [12].

The microwave spectrum and structure for butadiene iron tricarbonyl were published in 1992 [13], followed by a more complete paper in 1993 [14] which included multiple isotopologues and the complete structure. An x-ray structure which did not show the hydrogen atoms was published by Mills and Robinson in 1963. [15] The microwave spectrum and structure for ruthenium tetracarbonyl dihydride were published in 1998. [16] For this dihydride complex the ruthenium atom is 0.28 Å from the center of mass, so individual spectra from the most abundant isotopologues are partially resolved. For the present work on butadiene ruthenium tricarbonyl, the ruthenium atom is only 0.04 Å from the center of mass so spectra from the isotopologues that do not have a nuclear spin I > 1/2, ^{96}Ru, ^{98}Ru, ^{102}Ru and ^{104}Ru, are only partially resolved. The most abundant isotopes of ruthenium are: ^{100}Ru (12 %), ^{101}Ru (17 %), ^{102}Ru (32 %) (strongest signals) and ^{104}Ru (18 %). The calculated structure for this complex is shown in Fig. 1. Analysis of the quadrupole hyperfine structure on the ^{101}Ru (I = 5/2) and ^{99}Ru (I = 5/2) rotational transitions provided the first molecular gas-phase ^{101}Ru and ^{99}Ru quadrupole coupling interaction strengths.

2. Experimental

2.1. Synthesis of the butadiene ruthenium tricarbonyl sample

The compound, (η^4-1,3-butadiene)Ru(CO)$_3$ (**1**) was prepared by a

* Corresponding author.
E-mail address: kukolich@arizona.edu (S.G. Kukolich).

https://doi.org/10.1016/j.jms.2024.111949
Received 2 August 2024; Received in revised form 13 September 2024; Accepted 23 September 2024
Available online 24 September 2024

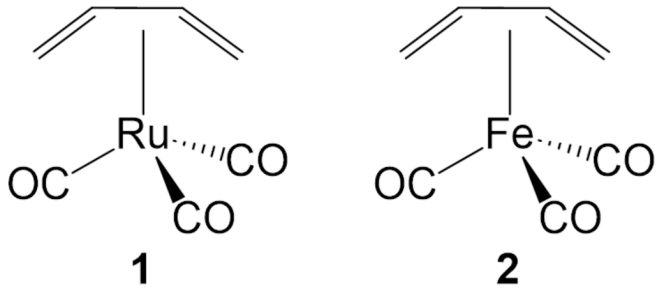

Fig. 1. Basic structures for (η^4-1,3-butadiene)$Ru(CO)_3$ –> Ru complex **1** and (η^4-1,3-butadiene)$Fe(CO)_3$ –> Fe complex **2**.

modification of a literature procedure [10]. This compound and the Fe containing congener (**2**) are shown in Fig. 1.

Chemicals were purchased from TCI, Oakwood Chemical, Sigma-Aldrich, or Fisher Scientific and used as obtained unless otherwise described. After being purified with an MBraun MS–SP solvent system, hexane was stored under N_2 with activated 3 Å molecular sieves. Ethylene gas was ordered from Airgas and used without further purification. All reactions were carried out under an N_2 atmosphere unless otherwise stated. Photochemical reactions used a custom-built light source with four 10-watt blue LEDs (455 nm, Pan Pan Supermarket) and four 10-watt UV LEDs (365 nm, JSTRONIC).

The compound $Ru_3(CO)_{12}$, (0.2995 g, 0.4684 mmol) in mixed hexanes (450 mL) was transferred to a 500 mL Schlenk flask. The mixture was purged with ethylene for roughly 10 min while stirring and then irradiated with 455 nm blue LEDs until it turned from orange to colorless. Irradiation was then switched to 365 nm UV light and continued for 1–2 h. Ethylene gas was continuously bubbled into the mixture during the whole irradiation process.

The UV irradiation process was monitored with IR until 90 % of the $(C_2H_4)Ru(CO)_4$ intermediate was converted to $(C_2H_4)_2Ru(CO)_3$. Then 9 mL of a saturated solution of 1,3-butadiene in hexanes was immediately added to the mixture. The reaction mixture was connected to a Schlenk line, the solution was purged with N_2 to replace the remaining ethylene, and the reaction mixture was stirred overnight. The fully reacted mixture was concentrated to around 20 mL under rotary evaporation and then filtered through a pad of alumina, which was then rinsed with 300 mL of pentane. The solvent was removed by rotary evaporation and the residue was further purified by column chromatography on alumina with pentane as the eluant to obtain the product as a colorless liquid in 38 % yield. The compound was identified by comparison with literature data [17]. ^{1}H NMR (400 MHz, $CDCl_3$): δ 5.49 (1H, m), 1.82 (1H, m), 0.46 (1H, m). IR (Hexanes): 2069, 2003, 1993 cm^{-1}.

2.2. Microwave Spectra

Rotational transitions of the Ru complex **1** were measured using a Flygare-Balle type pulsed-beam Fourier transform microwave spectrometer [1] in the region of 5–15 GHz. This spectrometer has the molecular beam perpendicular to the cavity axis. The diluted mixtures of the Ru complex **1** in argon under 1 atm of backing pressure were produced by placing the sample in a glass sample cell that allowed small amounts of sample to be picked up in the argon stream and pulsed into the microwave cavity in the vacuum chamber.

Ru complex **1** is known to be air and moisture sensitive. We found it was necessary to purge our gas-handling system with argon three times using a liquid nitrogen trap with the goal of eliminating any water coating the walls of our tubing that joins our sample cell to the spectrometer gas manifold. The compound was cooled to a constant 15 °C while on the spectrometer using a Peltier thermoelectric cooling system. Using a diffusion pump, a pressure range of 10^{-6} – 10^{-7} torr was maintained inside the spectrometer cavity before each gas pulse. Ru complex **1**, in 0.8 atm of ultrapure argon, was pulsed into the chamber at a frequency of 2 Hz using a General Valve series 9 pulsed valve. Frequency scans of up to 100 MHz were made in regions where strong rotational transitions were predicted from the calculations. A Labview program controlled the spectrometer for the stepwise scans and a Matlab program was used to visualize the scans. After transitions were located, data was collected at fixed frequencies within 1 MHz of the transitions. Details of the homodyne signal capture microwave circuit have been published earlier.[1] Briefly, 4 short (1 microsecond) pulses that are separated by 100 microseconds are generated using a NI 6602 Counter/Timer card and sent to a fast switch coupled to the microwave cavity. The echo signal from the homodyne mixer is sent to a preamplifer and mixed down using the stimulation signal. The mixed signal is sent to a preamplifier and digitized at 3.125 MHz using a picoscope digitizer. The signal is processed in our software to add the four free induction decay signals together. Each step in the scan contained 300 valve pulses that contain 1200 free induction decay signals.

An example of the recorded spectrum with the stimulating microwave frequency of 8433.8 MHz is shown in Fig. 2. The multiple peaks are due to the different isotopes of ruthenium and splitting due to ruthenium quadrupole coupling. The ^{99}Ru (12.8 %) and ^{101}Ru (17.1 %) isotopes have nuclear spin 5/2 and nuclear quadrupole moments and hyperfine structure splittings near the strongest isotope are not completely resolved in this spectrum.

3. Computational

Calculations were performed on the University of Arizona HPC system using Gaussian G-16[18] with 94 cores and 512 GB of memory per node, as described earlier[19]. Calculations focused on methods that have been shown to predict the gas phase structures of complexes and include DFT with functionals B3LYP, [20] DEF2, M11, [21] and MP2 [22]. Basis sets used include: Def2(Aldrichs/Weigend) and aug-cc-pVQZ (Dunning). For some calculations, core potentials (ECP) and all electron (AE) basis sets for ruthenium from the Basis Set Exchange[23] were used for calculations. Calculations were first done on (η^4-butadiene)$Fe(CO)_3$ (**2**) to test the various basis sets, since experimental rotational constants are available for this complex. The results for Fe complex **2** are shown in Table 1. Calculations were done with normal basis sets and with extended core potential (ECP from the Basis Set Exchange (BSE) [24]) for both the Fe and Ru calculations. The ECP basis used for Fe was from Balbanov, et al.[14] The ratios of the calculated (B3LYP) to experimental rotational constants were used to calculate scaling factors to use with the Ru complex **1** calculations to predict transition frequencies.

A summary of the predicted rotational constants and experimentally determined constants for Ru complex **1** are given in Table 2. The G-16 – Dunning (cc-pV) basis sets do not include ruthenium, so the Aldrichs/Weigend (def2) basis sets, which include ECP, were used for the Ru complex **1** calculations (basis set 1). Very similar results were obtained for Fe complex **2** for the Dunning (cc-pV) and def2 basis sets. One ECP used for Ru complex **1** was from Peterson, et al. [25] The calculations in Table 2 all involve core potentials (ECP).

The calculated, scaled rotational constants B and C in the last column of Table 2 are within a few MHz of the experimental values. Both Fe complex **2** and Ru complex **1** have a and c – axis dipole components. The Ru complex **1** structure from the B3LYP/def2qzvpp calculation (column 3 – Table 2.) is shown in Fig. 3. The Cartesian coordinates for all atoms in this calculation are given in Table 3.

Further calculations to predict quadrupole coupling strengths using ECP and "all-electron" basis sets from the BSE [14] are given in Table 4. We note that the Ru complex quadrupole coupling values using the ECP (column 2) give much smaller χ – values than obtained from the all-electron calculations. The rotational constants from AE calculations are in poor agreement with experimental values. Since the all-electron (AE) calculations with optimization give significantly smaller rotational constants, the geometry was fixed at the coordinates obtained

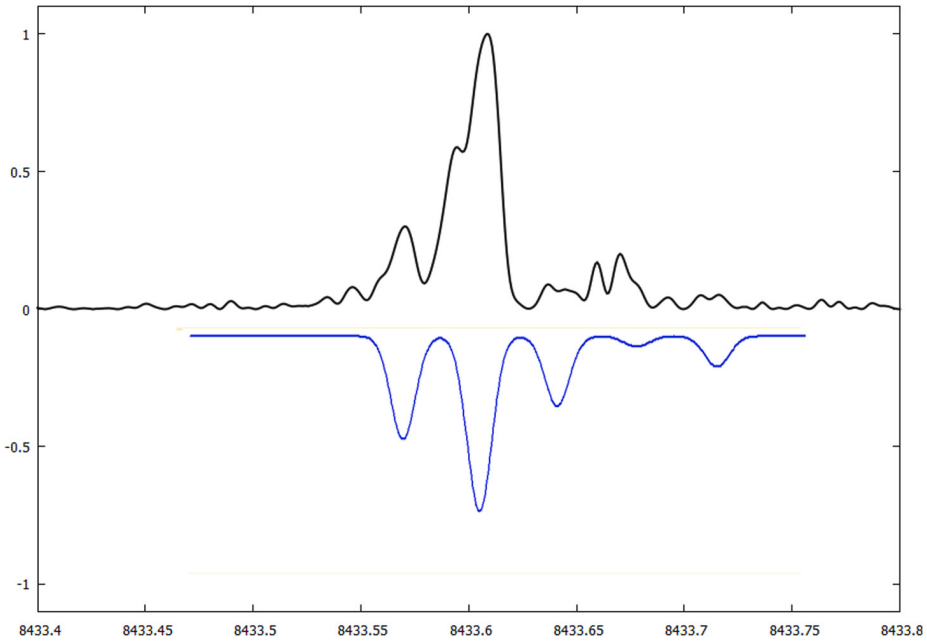

Fig. 2. Direct measurement of the $5_{24} \rightarrow 4_{23}$ transition of (η^4-butadiene)Ru(CO)$_3$ (**1**) with a microwave stimulation frequency of 8433.8 MHz. Frequency scale is in MHz. The line center of the largest peak is 8433.607 MHz. The lower trace is a simulation using line frequencies calculated for the isotopes of ruthenium, ^{104}Ru, ^{102}Ru, ^{100}Ru, and ^{96}Ru, with intensities proportional to the natural abundances of the isotopes. Possible quadrupole components from ^{99}Ru and ^{101}Ru are not included in the simulation.

Table 1
Calculations on Fe complex **2**. Some calculations used ECP for Fe – aug-cc-pVQZ[14].

Method	Experiment	B3LYP	B3LYP	MP2	M11	B3LYP
Basis set		1	2	3	3	4
A	1005.4201(3)	1003.2	1003.6	1237.3	1005.0	1003.2
B	958.0408(2)	954.9	954.6	985.8	983.7	954.9
C	933.6865 (3)	922.0	922.0	967.7	937.5	921.9
A factor			1.001797			
B factor			1.003600			
C factor			1.012706			

Basis sets: 1. def2-QZVPP, 2. aug-cc-pVQZ, 3. def2-QZVPP. 4. def2-QZVPP (C,H, O) – ECP Fe aug-cc-pVQZ. A-factor, B-factor and C-factor are the scaling factors to multiply calculated constants by to obtain experimental values. Units are MHz.

from the ECP calculation (column 2) and single point calculations were performed to determine quadrupole coupling constants for all the (AE) calculations in Table 4.

4. Analysis of the spectra

Predictions of the microwave spectrum were made using the microwave analysis suite from Herb Pickett – SPCAT [2] program available from the JPL website. Wide scans were conducted with the molecular source held at 0° C at the expected a-dipole transition frequency of $5_{05} \rightarrow 4_{04}$ predicted to be at 8356 MHz for the most abundant isotopologue based on scaled B3LYP/aug-cc-pVQZ calculations. No signals were observed and the temperature was increased to 15° C. The scan at this temperature, using the same scan region, detected a signal at 8433.607 MHz. The signal was tentatively assigned to be at $5_{05} \rightarrow 4_{04}$ and a scan for the $4_{04} \rightarrow 3_{03}$ transition predicted at 6696 MHz was performed. No signals were detected and the 8433.607 MHz signal was no longer present. The liquid sample changed color to a yellowish hue. We loaded a second sample and the signal at 8433.607 returned and a scan of 8433 – 8468 MHz was performed. A signal at 8460.0831 MHz was detected and based on this result a scan of 8433 down to 8281 was conducted. A signal was detected at 8370.207 MHz and we reassigned the two signals near 8.4 GHz. Based on the two transitions at 8433.607 MHz (initially reassigned to $5_{14} \rightarrow 4_{13}$) and 8370.207 MHz (newly assigned to $5_{05} \rightarrow 4_{04}$), a tentative fit was performed while holding the rotational constant A fixed to the scaled predicted value of 936.8 MHz using SPFIT [2].

Table 2
Ru complex **1** calculations. The calculations in column 3 used ECP for Ru – aug-cc-pVQZpp. The units are MHz. Dipole moments in Debye. H is Hartrees.

Method	Experiment	B3LYP	B3LYP	MP2	M11	B3LYP	B3LYP	PBE0	SCALED B3LYP
Basis set		1	2	3	4	5	6	7	8
A	932.20113(4)	938.6	935.1	976.9	940.2	934.8	935.0	959.6	940.3
B	858.0317(5)	852.3	848.5	864.2	872.4	848.7	849.1	875.9	855.3
C	831.3520(4)	823.2	819.8	859.4	841.6	820.1	820.1	847.9	833.7
μ_A		2.2		−3.1	−1.7	−2.2	−2.3	−2.0	
μ_B		0		0	0	0	0	0	
μ_C		0.8		−0.8	−0.9	−0.8	−0.8	−0.8	
Energy (H)			−590.971	−589.744	−590.865	−590.932	−590.895	−590.265	

Basis sets: 1. def2-QZVPP(ECP), 2. aug-cc-pVQZ (C,H,O) ECP Ru – aug-cc-pVQZpp, 3. def2-TZVPP, 4. def2-TZVPP, 5. cc-pVTZ (C,H,O) – ECP Ru – aug-cc-pVQZpp, 6. 6–311++G** (C,H,O) ECP Ru – aug-cc-pVQZpp 7. def2QZVPP, 8. Scaled values using column 3 of Table 2.

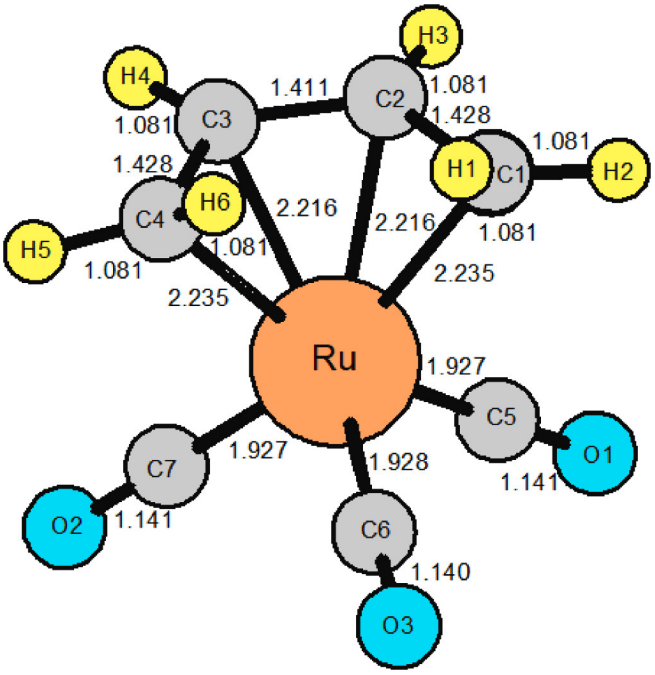

Fig. 3. Optimized structure of Ru complex **1** using B3LYP/def2-QZVPP. Bond distances in Angstrom units (Å).

Table 3
Cartesian coordinates (Å) for all atoms in Ru complex **1**, in the COM system. From the B3LYP/def2qzvpp calculation.

ATOM	a	b	c
H1	−1.59439	2.44935	0.39670
H2	−2.23434	1.03785	1.33455
H3	−2.04038	1.24000	−1.73964
C1	−1.74415	1.37963	0.43431
C2	−1.98365	0.70590	−0.80155
C3	−1.98348	−0.70558	−0.80227
C4	−1.74376	−1.38049	0.43291
H4	−2.04006	−1.23875	−1.74089
H5	−2.23404	−1.03976	1.33350
H6	−1.59369	−2.45013	0.39422
O1	1.68498	2.22622	−1.21869
O2	1.68560	−2.22461	−1.22074
O3	1.10632	−0.00136	2.84150
C5	1.05278	1.38826	−0.77179
Ru	−0.04051	0.00001	−0.00310
C6	0.70852	−0.00081	1.77346
C7	1.05314	−1.38723	−0.77310

A scan of 10052–10144 MHz detected signals that could be assigned to $6_{16} \rightarrow 5_{15}$ (10026.1971 MHz), $6_{06} \rightarrow 5_{05}$ (10030.5575 MHz), and $6_{25} \rightarrow 5_{24}$ (10110.1460 MHz). By fitting these four assigned transitions to A, B, and C, predictions were made for other transitions. Based on these assignments, the signal at 8433.607 MHz was reassigned to $5_{24} \rightarrow 4_{23}$. Signals were found near the predicted transitions, and more measurements were made to refine the rotational constants. In total, 26 measured rotational frequencies were used to fit A, B, C, D_J using the S-reduced Hamiltonian, 22 a-dipole transitions and 4c-dipole transitions. The assigned transitions and the errors are given in Table 5, and the experimental rotational and distortion constants for ^{102}Ru, ^{101}Ru, and ^{99}Ru, are given in Table 6.

The quadrupole coupling constants were calculated with Gaussian 16 using the optimized structure with B3LYP and the def2-QZVPP(ECP) basis set and several other basis sets. The results are summarized in Table 4. Line frequency predictions were made using the calculated values of the coupling constants for ^{101}Ru (I = 5/2) and ^{99}Ru (I = 5/2) with SPCAT.[2] Short scans with 300 pulse cycles per frequency step (~200 kHz) were performed to map the quadrupole coupling splitting around the J = 5 → J = 4 and K = 0 at 8370 +/- 20 MHz and J = 4 → J = 3 and K = 0 at 6709 +/- 20 MHz. Several weak signals were observed and assigned using the predicted spectrum to obtain a tentative fit using SPFIT for ^{101}Ru. Based on the preliminary fit, several lines were predicted at J = 3 → J = 2 at K_a = 0 and 1 and were observed and measured. A total of 16 transitions were measured and fit with σ = 8 kHz with minimal change to the rotational constants A, B and C. This is expected given that ruthenium is very close to the center of mass. Additional signals were observed in the spectrum very close to ^{101}Ru transitions. Using the fit produced for ^{101}Ru, the unassigned transitions were quickly assigned to the ^{99}Ru isotope. 18 transitions were fit to 20 kHz using A, B, C and $1.5\chi_{aa}$ and $0.25(\chi_{bb}\text{-}\chi_{cc})$. The results of fitting the measured transitions are shown in Tables 6, 7, and 8. Observed transitions for ^{101}Ru and ^{99}Ru are shown in Fig. 4.

5. Discussion

The observed rotational transitions were fitted to rotational and distortion constants shown in Table 6 and are very similar to calculated values for Ru complex **1**. The ruthenium isotopic splitting could be observed as seen in Fig. 2. The splittings between ruthenium isotopes without nuclear spin are small because ruthenium is close to the center of mass, and thus changing its mass does not greatly affect the moments of inertia. The central peak has been assigned to the ^{102}Ru isotope, although both the ^{99}Ru and ^{101}Ru contain one component unresolved in the central peak (predicted frequencies are within 20 kHz of ^{102}Ru prediction for K_a = 0). ^{101}Ru has splittings greater than 50 MHz for J = 5 → J = 4 and ^{99}Ru has splittings of 10 MHz. The signals observed in Fig. 4, 600 kHz from the central peak, is due to the quadrupole coupling splittings of each nucleus ^{99}Ru and ^{101}Ru. The quadrupole hyperfine structure for ^{99}Ru and ^{101}Ru was well resolved and transitions with ΔF = +1 were observed at three J values with transitions given in Tables 7 and 8. The fitted χ_{aa}, χ_{bb} and χ_{cc} values for each isotope are given in Table 6. We note that taking the ratio of χ_{aa} for ^{101}Ru toχ_{aa} ^{99}Ru gives 5.77(26), a value that is within the experimental values of the ratio of quadrupole moments of Pyykkö[26] of Q (^{101}Ru) / Q (^{101}Ru) equal to 5.78(41).

The calculated optimized structures for Ru complex **1** and Fe complex **2** can be compared to look for possible structural effects of the metal identity. The structures were optimized using B3LYP/def2-QZVPP. The optimized structure of Ru complex **1** showed a butadiene-ruthenium distance of 1.755 Å. The optimized structure of Fe complex **2** had a butadiene-iron distance of 1.625 Å. The greater distance between the metal and butadiene ligand in the ruthenium complex can be attributed to the greater size of the ruthenium atom compared to iron.

Previous ^{13}C NMR experiments on Ru complex **1**, Fe complex **2**, and butadieneOs$(CO)_3$ [27] found that one of the terminal hydrogens of butadiene is pushed away from the metal atom and outside of the butadiene plane to a greater extent when the metal is ruthenium instead of iron. The optimized structures of the gas-phase ruthenium and iron complexes using B3LYP/def2-QZVPP support these observations from ^{13}C NMR. The dihedral angle *C*2-C3-C4-H6 from Fig. 3 is 44.07° for the ruthenium complex. The same angle for the iron complex was calculated to be 42.82°. The increasing angle with ruthenium compared to iron has been attributed to increasing sp^3 character in the terminal carbons of the butadiene ligand.

For Fe complex **1**, the calculated barrier to internal rotation of the Fe$(CO)_3$ group was 3951 cm^{-1} using B3LYP/LANL2DZ. For the ruthenium complex, the barrier was calculated to be 6145 cm^{-1} using the same method and basis set. These are crude approximate barrier calculations since the Ru complex **1** dissociates with internal rotation. It was noted that Ru complex **1** is much less stable than Fe complex **2**.

Table 4
Ru complex **1** quadrupole calculations. The calculations in column 2 used ECP for Ru – aug-cc-pVQZpp[15] column 3', for comparison. All other calculations were done with all-electron (AE) from BSE. The quadrupole coupling terms (6—7) are for the ^{101}Ru isotopologues, and rows 8–9 are quadrupole terms for ^{99}Ru isotopologues. Frequencies are in MHz, dipole moments in Debye, H is Hartrees.

Method	1. Experiment	2. B3LYP/ECP	3. B3LYP/AE	4. B3LYP/AE	5. B3LYP/AE	6. B3LYP/AE/DKH	7. B3LYP/AE/DKH	8. B3LYP/AE/DKH
Basis set		2	3	4	5	6	7	8
A	932.2011(4)	935.1	938.6	938.6	938.6	938.7*	938.6	938.0
B	858.0317(4)	848.5	852.26	852.26	852.26	852.03	852.26	852.26
C	831.3520(4)	819.8	823.21	823.21	823.21	823.06	823.21	823.20
$3/2*\chi_{aa}$ ^{101}Ru	98.14(17)	3.62	129.086	108.09	108.27	120.20	108.08	129.09
$1/4*(\chi_{bb}-\chi_{cc})$ -^{101}Ru	36.05(3)	3.41	43.30	40.37	40.50	41.96	40.858	43.297
$3/2*\chi_{aa}$ ^{99}Ru	17.1(8)		21.98	18.407	18.439		18.41	21.98
$1/4*(\chi_{bb}-\chi_{cc})$ ^{99}Ru	6.2(3)		7.37	6.875	6.897		6.96	7.37
μ_A		2.2	2.6	2.1	2.13	2.1	2.1	2.6
μ_B		0.0	0.0	0.0	0.0	0.0	0.0	0.0
μ_C		−0.8	0.88	−0.8	0.81	0.8	−0.81	0.88
Energy (H)			−5026.21	−4940.19	−4940.18	−5026.39	−4940.15	−5026.22

Basis sets used: 2. ECP Ru – aug-cc-pVQZpp 3. aug-cc-pVTZ-DK, ANO-DK3 4. ANO-RCC-VQZP 5. ANO-RCC-VDZP for Ru, and for H,C,O aug-cc– 6. calculation using an all-electron basis set cc-pVTZ-DK from BSE in uncontracted form plus DKH relativistic Hamiltonian. Calculation done on previously optimized geometry with def2-QZVP integral=(UncontractAO,DKH,grid = 599590) 7. aug-cc-pVTZ-DK 8. ANO-DK3 integral=(UncontractAO,DKH,grid = 3500590) scf = novaracc 8. ANO-DKH −integral=(UncontractAO,DKH,grid = 3500590) scf = novaracc

Table 5
Results of the SPFIT least-squares fit of 26 measured rotational frequencies for ^{102}Ru complex **1**. Rotational and distortion constants are given in Table 6 and were used to determine the observed minus calculated (Obs-calc) deviations.

J'_{KaKc}	J''_{KaKc}	Measured frequency (MHz)	obs-calc (kHz)	Dipole
3_{13}	2_{12}	5024.7095	−5.0	a
3_{03}	2_{02}	5045.9091	−3.1	a
3_{12}	2_{11}	5103.8920	3.7	a
4_{14}	3_{13}	6694.3164	−1.5	a
4_{04}	3_{03}	6709.9235	3.6	a
4_{23}	3_{22}	6752.7952	4.9	a
4_{13}	3_{12}	6796.0133	0.6	a
5_{15}	4_{14}	8361.2233	−7.5	a
5_{05}	4_{04}	8370.2075	2.6	a
5_{24}	4_{23}	8433.6071	0.6	a
5_{33}	4_{32}	8460.0831	10.8	a
5_{14}	4_{13}	8478.3747	−3.7	a
6_{16}	5_{15}	10026.1971	3.0	a
6_{06}	5_{05}	10030.5937	0.0	a
6_{25}	5_{24}	10110.1460	2.2	a
6_{15}	5_{14}	10148.9102	−13.3	a
7_{17}	6_{16}	11689.9519	−13.1	a
7_{07}	6_{06}	11691.9375	14.6	a
7_{26}	6_{25}	11782.4673	−12.0	a
8_{18}	7_{17}	13353.1071	8.5	a
8_{08}	7_{07}	13353.9257	7.5	a
9_{09}	8_{08}	15016.2455	−5.0	a
3_{30}	2_{20}	5503.9665	1.1	c
3_{31}	2_{21}	5509.0959	1.1	c
4_{40}	3_{30}	7370.6275	−1.3	c
4_{41}	3_{31}	7371.3953	1.4	c

Table 6
Rotational constants and distortion constants obtained from the least-squares fitting of 16 transitions for ^{101}Ru and 18 transitions for ^{99}Ru complex **1**. The standard deviation of the fit is 7.9 kHz and 20 kHz respectively.

Isotope	^{102}Ru	^{101}Ru	^{99}Ru
A	932.20099(42)	932.186(13)	932.25(15)
B	858.03248(47)	858.03300(91)	858.040(11)
C	831.35161(37)	831.35341(44)	831.3512(49)
d_J (kHz)	0.0862(29)	[0.0862]*	[0.0862]*
$1.5\chi_{aa}$	–	98.14(17)	17.05(77)
$0.25(\chi_{bb}-\chi_{cc})$	–	36.054(29)	6.22(32)
χ_{aa}	–	65.43(11)	11.33(51)
χ_{bb}	–	39.39(08)	6.8 (1.4)
χ_{cc}	–	−104.82(08)	−18.1(1.4)
σ for fit (kHz)		7.9	20.

*d_J values for ^{101}Ru and ^{99}Ru were fixed at values from the ^{102}Ru fit.

Table 7
Results of the SPFIT least-squares fit of 16 measured rotational frequencies for ^{101}Ru complex **1**. Rotational and quadrupole coupling constants are given in Table 6 and were used to determine the observed minus calculated (Obs-calc)(o-c) deviations.

J'_{KaKc}	2F'	J''_{KaKc}	2F"	Measured frequency (MHz)	o-c (kHz)
3_{13}	11	2_{12}	9	5021.674	−10.3
3_{13}	7	2_{12}	5	5029.89	−3.1
3_{13}	5	2_{12}	3	5033.085	11.1
3_{03}	11	2_{02}	9	5042.947	9.9
3_{03}	9	2_{02}	7	5046.572	14.8
3_{03}	7	2_{02}	5	5050.654	−10.8
4_{14}	11	3_{13}	9	6693.745	5.7
4_{14}	13	3_{13}	11	6692.186	−3.5
4_{04}	13	3_{03}	11	6707.212	5.9
4_{13}	13	3_{12}	11	6794.383	−0.2
4_{13}	11	3_{12}	9	6797.864	−6.1
5_{15}	13	4_{14}	11	8360.691	2.6
5_{05}	15	4_{04}	13	8368.083	−1.4
5_{05}	11	4_{04}	9	8372.253	−13.7
5_{24}	7	4_{23}	5	8433.269	2.6
5_{14}	15	4_{13}	13	8476.328	2.2

Table 8
Results of the SPFIT least-squares fit of 18 measured rotational frequencies for ^{99}Ru complex 1. Rotational and quadrupole coupling constants are given in Table 6 and were used to determine the observed minus calculated (Obs-calc) or (o-c) deviations.

J'_{KaKc}	2F'	J''_{KaKc}	2F"	Measured frequency (MHz)	o-c (kHz)
3_{13}	1	2_{12}	1	5024.0000	23.9
3_{13}	11	2_{12}	9	5024.2061	8.9
3_{13}	9	2_{12}	7	5024.7322	23.4
3_{03}	11	2_{02}	9	5045.4153	−1.5
3_{03}	7	2_{02}	7	5046.0125	−17.8
3_{03}	9	2_{02}	7	5046.0223	−8.2
3_{03}	7	2_{02}	5	5046.7468	−11.5
3_{03}	5	2_{02}	3	5047.0970	−6.6
4_{14}	13	3_{13}	11	6693.9074	−51.2
4_{14}	9	3_{13}	7	6694.7510	6.8
4_{14}	5	3_{13}	3	6695.0156	3.8
5_{05}	13	4_{04}	11	8370.2075	−12.8
5_{05}	11	4_{04}	9	8370.5890	13.3
5_{05}	9	4_{04}	7	8370.7382	6.3
5_{15}	15	4_{14}	13	8360.9097	−44.8
5_{15}	13	4_{14}	11	8361.1585	11.4
5_{24}	7	4_{23}	5	8433.5945	14.2
6_{06}	15	5_{05}	13	10030.5662	0.2

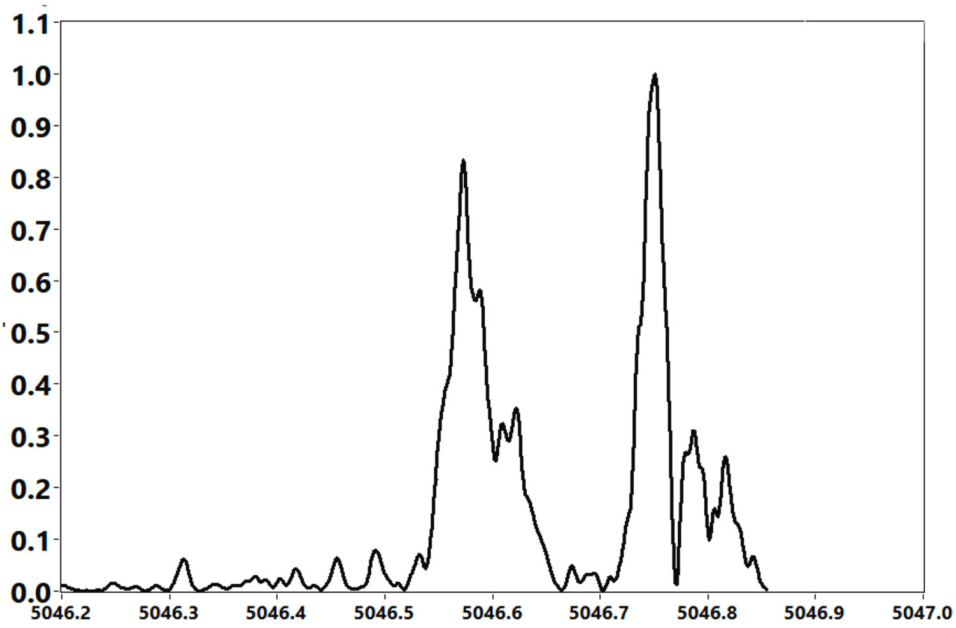

Fig. 4. Quadrupole coupling hyperfine components for ^{99}Ru, (F' = 9/2 to F"=7/2), $3_{03} - 2_{02}$ transition at 5046.572 MHz and the ^{101}Ru (F'= 7/2 to F"= 5/2), $3_{03} - 2_{02}$ transition at 5046.747 MHz. These data were obtained with 300 cycles.

6. Conclusions

Precise and accurate rotational constants were combined with high-level calculations to provide the first detailed structure information for (η^4-butadiene)Ru(CO)$_3$. G-16, ECP calculations with B3LYP/def-QZVPP provided rotational constants in very good agreement with experimental values. Large basis all electron calculations provided good predictions of the ^{101}Ru and ^{99}Ru quadrupole coupling strengths and facilitated measurements for the ^{101}Ru and ^{99}Ru quadrupole coupling parameters. The values obtained are $1.5\chi_{aa} = 98.14(17)$ MHz and $0.25(\chi_{bb}\text{-}\chi_{cc}) = 36.054(29)$ for ^{101}Ru in reasonable agreement with AE calculated values. Measured hyperfine structure splittings for ^{99}Ru quadrupole coupling yielded the values of $1.5\chi_{aa} = 17.05(77)$ MHz and $0.25(\chi_{bb}\text{-}\chi_{cc}) = 6.22(32)$ MHz. Values calculated using ECP for Ru are much smaller, as expected.

CRediT authorship contribution statement

Adam M. Daly: Writing – review & editing, Writing – original draft, Validation, Software, Methodology, Investigation, Formal analysis, Data curation. **Kristen K. Roehling:** Writing – review & editing, Writing – original draft, Visualization, Validation, Software, Investigation, Formal analysis, Data curation. **Rhett P. Hill:** Writing – review & editing, Visualization, Validation, Investigation. **Myla G. Gonzalez:** Writing – review & editing, Visualization, Validation, Investigation, Data curation. **Xin Kang:** Writing – review & editing, Validation, Resources, Methodology, Investigation. **Lisa McElwee-White:** Writing – review & editing, Writing – original draft, Validation, Supervision, Resources, Project administration, Methodology, Funding acquisition, Formal analysis. **Stephen G. Kukolich:** Writing – review & editing, Writing – original draft, Visualization, Validation, Supervision, Software, Project administration, Funding acquisition, Formal analysis, Data curation, Conceptualization.

Declaration of competing interest

The authors declare that they have no known competing financial interests or personal relationships that could have appeared to influence the work reported in this paper.

Data availability

Data will be made available on request.

Acknowledgements

This material is based upon work supported by the National Science Foundation under Grant No. CHE-1952289 at the University of Arizona. Synthesis was supported by the National Science Foundation under Grant No. DMR-2216070 at the University of Florida. We are very grateful to Fernando Clemente and Doug Fox from Gaussian, Inc. for much help with the calculations.

References

[1] B.S. Tackett, C. Karunatilaka, A.M. Daly, S.G. Kukolich, Organometallics 26 (8) (2007) 2070–2076, https://doi.org/10.1021/om061027f.
[2] H.M. Pickett, The fitting and prediction of vibration-rotation spectra with spin interactions, J. Mol. Spectrosc. 148 (2) (1991) 371–377, https://doi.org/10.1016/0022-2852(91)90393-O.
[3] O.-K. Kwon, J.-H. Kim, H.-S. Park, S.-W. Kang, Atomic Layer Deposition of Ruthenium Thin Films for Copper Glue Layer, J. Electrochem. Soc. 151 (2) (2004) G109.
[4] C.C. Yang, S. Cohen, T. Shaw, P.C. Wang, T. Nogami, D. Edelstein, Characterization of "Ultrathin-Cu"/Ru(Ta)/TaN Liner Stack for Copper Interconnects, IEEE Electron Device Lett. 31 (7) (2010) 722–724.
[5] D. Gall, The search for the most conductive metal for narrow interconnect lines, J. Appl. Phys. 127 (5) (2020) 050901.
[6] C. Feit, U. Kumar, M.R. Islam, L. Tomar, S.N. Berriel, J.T. Gaskins, P.E. Hopkins, S. Seal, P. Banerjee, Surface treatment of TaN for sub-2 nm, smooth, and conducting atomic layer deposition Ru films, J. Vac. Sci. Technol. a. 42 (3) (2024) 032407.
[7] D.Z. Austin, M.A. Jenkins, D. Allman, S. Hose, D. Price, C.L. Dezelah, J.F. Conley Jr.,, Atomic Layer Deposition of Ruthenium and Ruthenium Oxide Using a Zero-Oxidation State Precursor, Chem. Mater. 29 (3) (2017) 1107–1115.
[8] Z. Gao, D. Le, A. Khaniya, C.L. Dezelah, J. Woodruff, R.K. Kanjolia, W.E. Kaden, T. S. Rahman, P. Banerjee, Self-Catalyzed, Low-Temperature Atomic Layer Deposition of Ruthenium Metal Using Zero-Valent Ru(DMBD)(CO)$_3$ and Water, Chem. Mater. 31 (4) (2019) 1304–1317.
[9] Y.W. Song, J. Lee, K. Lee, Y. Lee, H.K. Jang, Atomic layer deposition of Ru by using a new Ru precursor, ECS Trans. 2 (4) (2006) 1–11, https://doi.org/10.1149/1.2204812.
[10] C.R. Brewer, N.C. Sheehan, J. Herrera, A.V. Walker, L. McElwee-White, Photochemistry of (η^4-diene)Ru(CO)$_3$ Complexes as Precursor Candidates for Photoassisted Chemical Vapor Deposition, Organometallics. 41 (6) (2022) 761–775, https://doi.org/10.1021/acs.organomet.1c00715.

[11] B.F. Hallam, P.L. Pauson, Metal derivatives of conjugated dienes. Part I. Butadiene- and cyclohexadiene-iron tricarbonyls, J. Chem. Soc. (1958) 642–645, https://doi.org/10.1039/JR9580000642.
[12] G. Wilkinson, M. Rosenblum, M.C. Whiting, R.B. Woodward, The Structure Of Iron Bis-Cyclopentadienyl, J. Am. Chem. Soc. 74 (8) (1952) 2125–2126, https://doi.org/10.1021/ja01128a527.
[13] S.G. Kukolich, M.A. Roehrig, G.L. Henderson, D.W. Wallace, Q.-Q. Chen, Microwave Measurements of the Rotational Spectrum of Butadiene Iron Tricarbonyl, J. Chem. Phys. 97 (2) (1992) 829, https://doi.org/10.1063/1.463185.
[14] S.G. Kukolich, M.A. Roehrig, D.W. Wallace, G.L. Henderson, Microwave Measurements of the Rotational Spectrum and Structure of Butadiene Iron Tricarbonyl, J. Am. Chem. Soc. 115 (5) (1993) 2021–2027, https://doi.org/10.1021/ja00058a058.
[15] O.S. Mills, G. Robinson, Studies of some carbon compounds of the transition metals. IV. The structure of butadiene irontricarbonyl, Acta Cryst. 16 (1963) 758–761, https://doi.org/10.1107/S0365110X63001973.
[16] T.G. Lavaty, P. Wikrent, B.J. Drouin, S.G. Kukolich, Microwave Measurements and Calculations on the Molecular Structure of Tetracarbonyldihydroruthenium, J. Chem. Phys. 109 (1998) 9473–9478, https://doi.org/10.1063/1.477608.
[17] S. Ruh, W. Von Philipsborn, Butadieneruthenium tricarbonyl. XIV., Carbon-13 NMR spectroscopy, J. Organomet. Chem. 127 (2) (1977) C59–C61, https://doi.org/10.1016/S0022-328X(00)89727-2.
[18] Frisch, M. J.; Trucks, G. W.; Schlegel, H. B.; Scuseria, G. E.; Robb, M. A.; Cheeseman, J. R.; Scalmani, G.; Barone, V.; Petersson, G. A.; Nakatsuji, H.; Li, X.; Caricato, M.; Marenich, A. V.; Bloino, J.; Janesko, B. G.; Gomperts, R.; Mennucci, B.; Hratchian, H. P.; Ortiz, J. V.; Izmaylov, A. F.; Sonnenberg, J. L.; Williams-Young, D.; Ding, F.; Lipparini, F.; Egidi, F.; Goings, J.; Peng, B.; Petrone, A.; Henderson, T.; Ranasinghe, D.; Zakrzewski, V. G.; Gao, J.; Rega, N.; Zheng, G.; Liang, W.; Hada, M.; Ehara, M.; Toyota, K.; Fukuda, R.; Hasegawa, J.; Ishida, M.; Nakajima, T.; Honda, Y.; Kitao, O.; Nakai, H.; Vreven, T.; Throssell, K.; Montgomery, J. A., Jr.; Peralta, J. E.; Ogliaro, F.; Bearpark, M. J.; Heyd, J. J.; Brothers, E. N.; Kudin, K. N.; Staroverov, V. N.; Keith, T. A.; Kobayashi, R.; Normand, J.; Raghavachari, K.; Rendell, A. P.; Burant, J. C.; Iyengar, S. S.; Tomasi, J.; Cossi, M.; Millam, J. M.; Klene, M.; Adamo, C.; Cammi, R.; Ochterski, J. W.; Martin, R. L.; Morokuma, K.; Farkas, O.; Foresman, J. B.; Fox, D. J., Gaussian 16, Revision C.01, Gaussian, Inc., Wallingford CT, 2016.
[19] J.L. Nichols, K.K. Roehling, A.M. Daly, S.G. Kukolich, Microwave measurements and calculations for the glyoxylic acid – Formic acid hydrogen-bonded complex, J. Mol Spectrosc. 395 (2023) 111806, https://doi.org/10.1016/j.jms.2023.111806.
[20] A.D. Becke, Density-functional thermochemistry. III. The role of exact exchange, J. Chem. Phys. 98 (1993) 5648–5652, https://doi.org/10.1063/1.464913.
[21] R. Peverati, D.G. Truhlar, Improving the Accuracy of Hybrid Meta-GGA Density Functionals by Range Separation, J. Phys. Chem. Lett. 2 (21) (2011) 2810–2817, https://doi.org/10.1021/jz201170d.
[22] Head-Gordon M.; People J. A.; Frisch M. J, MP2 energy evaluation by direct methods, Chem. Phys. Lett. 153 (6) (1998) 503–506, https://doi.org/10.1016/0009-2614(88)85250-3.
[23] N.B. Balabanov, K.A. Peterson, Systematically convergent basis sets for transition metals. I. All-electron correlation consistent basis sets for the 3d elements Sc-Zn, J. Chem. Phys. 123 (2005) 064107, https://doi.org/10.1063/1.1998907.
[24] B.P. Pritchard, D. Altarawy, B. Didier, T.D. Gibson, T.L. Windus, A New Basis Set Exchange: An Open, Up-to-date Resource for the Molecular Sciences Community, J. Chem. Inf. Model. 59 (11) (2019) 4814–4820, https://doi.org/10.1021/acs.jcim.9b0072.
[25] K.A. Peterson, D. Figgen, M. Dolg, H. Stoll, Energy-consistent relativistic pseudopotentials and correlation consistent basis sets for the 4d elements Y-Pd, J. Chem. Phys. 126 (2007) 124101, https://doi.org/10.1063/1.2647019.
[26] P. Pyykkö, Spectroscopic nuclear quadrupole moments, Molecular Physics 99 (19) (2001) 1617–1629, https://doi.org/10.1080/00268970110069010.
[27] S. Zobl-Ruh, W. Von Philipsborn, (Burtadiene)tricarbonylosmium synthesis and structural comparison with the Fe- and Ru-complexes based on ^{1}H- and ^{13}C-NMR, Spectroscopy. *Helv. Chim. Acta.* 63 (4) (1980) 773–779, https://doi.org/10.1002/hlca.19800630404.